

## Small-scale structures in the far-infrared background<sup>\*</sup>

Uwe Herbstmeier<sup>1</sup>, Péter Ábrahám<sup>1,2</sup>, Dietrich Lemke<sup>1</sup>, R.J. Laureijs<sup>3</sup>, Ulrich Klaas<sup>1,3</sup>, Kalevi Mattila<sup>4</sup>, Christoph Leinert<sup>1</sup>, Christian Surace<sup>1</sup>, and Michael Kunkel<sup>1</sup>

<sup>1</sup> Max-Planck-Institut für Astronomie, Königstuhl 17, D-69117 Heidelberg, Germany

<sup>2</sup> Konkoly Observatory of the Hungarian Academy of Sciences, P.O. Box 67, 1525 Budapest, Hungary

<sup>3</sup> ISO Science Operation Centre, Astrophysics Division, Space Science Department of ESA, Villafranca, P.O. Box 50727, E-28080 Madrid, Spain

<sup>4</sup> University of Helsinki, Observatory, P.O. Box 14, Tähtitorninmäki, FIN-00014 Helsinki, Finland

Received 22 September 1997 / Accepted 20 January 1998

**Abstract.** Four fields with areas ranging from 80 to 2000 arcmin<sup>2</sup> have been mapped with the photometer on board of the Infrared Space Observatory (ISO) at 90 and around 180  $\mu\text{m}$  in regions of bright and faint cirrus. We examined the spatial characteristics of the infrared background emission with high spatial resolution and found that the fluctuations in the background emission limit the detection sensitivity of ISOPHOT for most of our observations. At 90  $\mu\text{m}$  the power law relation between the power in the fluctuations and the spatial frequencies established from IRAS data could be extended to twice as high spatial frequencies. At 180  $\mu\text{m}$  the small-scale fluctuations were studied for the first time by a cold space telescope with arcminute-resolution. A similar power law and spectral index down to spatial scales of 3' as for the 90  $\mu\text{m}$  component is found. For cirrus clouds the spatial frequency spectrum in the far-infrared has a similar shape as that derived from 21 cm line observations of the interstellar neutral hydrogen. In faint regions the fluctuations are caused presumably by randomly distributed extragalactic sources. Future 3 m class space telescopes surveying the sky around 200  $\mu\text{m}$  will not be hampered by cirrus over most of the sphere.

**Key words:** methods: observational – ISM: structure – Infrared: ISM: continuum – diffuse radiation

### 1. Introduction

Low et al. (1984) introduced the term “galactic cirrus” for dust emission from irregularly shaped interstellar clouds which dominate the far-infrared sky at 60 and 100  $\mu\text{m}$ . This patchiness limits the reliable detection of faint infrared point sources. It also restricts the possibility to determine an extragalactic back-

ground, expected to be caused by a population of unresolved distant galaxies (e.g. Helou & Beichman (1990), Guiderdoni et al. (1997)).

To quantify the severity of these limitations Gautier et al. (1992) determined the noise produced by emission fluctuations along IRAS scans. The flux of a source is derived from the brightness difference between on-source ( $x$ ) and background positions. Frequently, two off-source positions at a distance  $\theta$  from the source are selected to correct for gradients in the background emission. But, background brightness fluctuations with scales of the order of  $\theta$  can distort the result. This uncertainty is estimated from a relative of the second order structure function of the sky brightness,  $B$ . This function  $S$  is the average difference squared for all possible on – off pairs in a given sky area:

$$S(\theta) = \langle |B(x) - \frac{B(x-\theta) + B(x+\theta)}{2}|^2 \rangle_x \quad (1)$$

The noise limit due to sky brightness fluctuations,  $N$ , is defined to be the flux density in the measurement aperture  $\Omega_{\text{aperture}}$ , which corresponds to the square root of  $S$  at the resolution limit  $\theta_{\text{min}}$ :  $N = S^{0.5}(\theta_{\text{min}}) \cdot \Omega_{\text{aperture}}$ . This “sky brightness structure noise” is called in the following briefly “structure noise”.

To predict the limiting structure noise for smaller scales and longer wavelengths than measurable with IRAS, Gautier et al. (1992) linked the expression for  $N$  to general spatial properties of the 100  $\mu\text{m}$  cirrus. As a measure for these spatial structures they calculate the values of the power,  $P$ , in brightness fluctuations on scale length,  $d$ , from the in-scan resolution limit of 2' up to the complete scan length. From a Fourier analysis of the brightness distributions the authors found the relation between  $P$  and the scale length or the corresponding spatial frequencies,  $d^{-1}$ :

$$P = P_0 \cdot \left(\frac{d_0}{d}\right)^\alpha \quad (2)$$

with the power  $P_0$  at a reference scale length  $d_0$ . Empirically a spectral index  $\alpha$  close to  $-3$  was found. Relating this general spatial characteristic of the cirrus to the function  $S$ , it is found that  $N$  decreases with improved resolution: On a scale length

---

Send offprint requests to: Uwe Herbstmeier (uherbst@mpia-hd.mpg.de)

<sup>\*</sup> Based on observations with ISO, an ESA project with instruments funded by ESA Member States (especially the PI countries: France, Germany, the Netherlands and the United Kingdom) and with the participation of ISAS and NASA

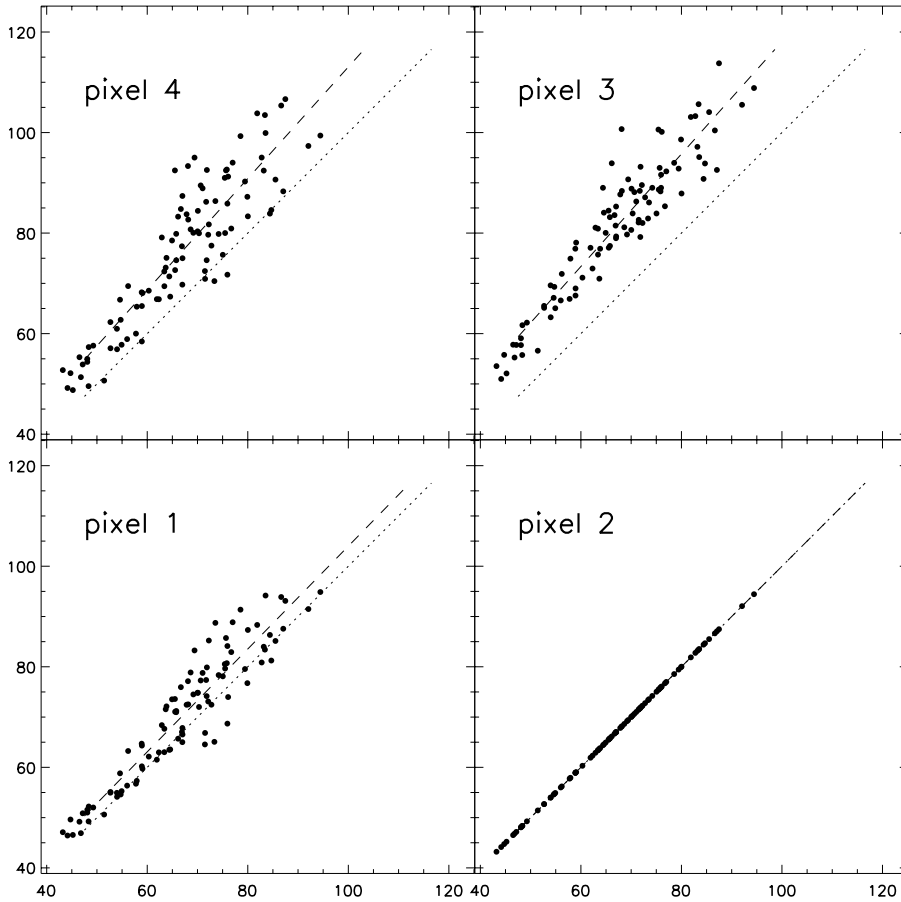


**Fig. 1.** C200 170 $\mu\text{m}$  measurements of the Cepheus filament as an example for the flat-fielding procedure. The brightness per raster point from each detector pixel  $i$  versus the brightness from pixel 2 is plotted. The dashed lines represent the fit to derive the flat field parameters. In the ideal case of no responsivity differences between the detector pixels all signals should scatter around the dotted lines. Deviations from the fitted line are due to small-scale brightness structures in the field and instrumental noise.

$d$  corresponding to the width of the measurement aperture the noise scales like:

$$N \propto \left(\frac{d}{d_0}\right)^{1-\frac{\alpha}{2}} \cdot P_0^{\frac{1}{2}} \quad (3)$$

Empirically, Gautier et al. (1992) found for cirrus clouds that the power  $P_0$  is proportional to  $\langle B \rangle^3$ , where  $\langle B \rangle$  is the mean brightness in the sky area. Helou & Beichman (1990) adopt this relation for all wavelengths of the dust emission replacing the mean brightness at 100  $\mu\text{m}$  with the spectrum of the source,  $B(\lambda)$ , and fix the index of the power law to the observed value of  $-3$ . With these assumptions they rewrite Eq. (3) to:

$$\frac{N_{\text{H\&B}}}{1 \text{ mJy}} = 0.3 \cdot \left(\frac{\lambda}{100 \mu\text{m}}\right)^{2.5} \left(\frac{D}{1 \text{ m}}\right)^{-2.5} \left(\frac{\langle B(\lambda) \rangle}{1 \text{ MJy sr}^{-1}}\right)^{1.5} \quad (4)$$

where the measurement aperture is identified with the resolution element of the telescope with diameter  $D$  at wavelength  $\lambda$ ,  $d \propto \frac{\lambda}{D}$  (see also Puget (1992)). This relation is widely used to plan observations of point sources, i.e. to select suitable fields or optimized observing strategies.

For ISOPHOT (Lemke et al. (1996)), the photometer on board of the Infrared Space Observatory ISO (Kessler et al. (1996)), the aperture size at 90  $\mu\text{m}$  is 46". Therefore, the validity of Eq. (3) can be tested for the improved resolution compared to IRAS (pixels size on sky: 3'  $\times$  5' (2.5')). Moreover, at 180  $\mu\text{m}$  ISOPHOT allows for the first time high resolution

studies of the spatial properties of the cirrus; although COBE's instrument DIRBE (Boggess et al. (1992)) extended the observable wavelength range beyond IRAS, the aperture size of 42' is much larger than the value for ISO of 1'.5 at 180  $\mu\text{m}$ .

In this paper we present ISOPHOT measurements which cover four fields of low and high sky brightness (Sects. 2 & 3). Three of them were observed at 90  $\mu\text{m}$  and all four were mapped in the new wavelength range around 180  $\mu\text{m}$ . We derive structure noise values and spatial frequency power spectra (Sects. 4 & 5). In Sect. 6 the results are compared with IRAS predictions and the characteristics of the interstellar gas. We discuss the influence on strategies for faint source observations with ISO and future space missions.

## 2. Observations

The four fields were taken out of different programs:

- 1, Cep, a filament in the Cepheus flare most probably at a distance of  $450 \pm 50$  pc (Kun (1997)). This region represents the bright cirrus component, comprising also molecular clouds.
- 2, HR, a faint filament in the direction of the star HR 6132. It is projected towards the boundary of the Draco nebula, a faint cirrus cloud at a distance of 600 pc (Herbstmeier et al. (1993)).
- 3, M03, a smooth area on the sky selected for studies of potential zodiacal light structures (Ábrahám et al. (1997)).

**Table 1.** Observational parameters and analysis results for the ISOPHOT observations of the four cirrus regions. Given are reference wavelength,  $\lambda_{\text{ref}}$ , information on the raster parameters, field size (also accounting for the pixel size) and exposure time,  $t_{\text{expo}}$ . The exposure time is the time spent observing one raster position. For non-oversampled rasters (M03\_90, M03\_180, NGP\_180) it corresponds to the measurement time per sky position. For maps oversampled in both dimensions (HR\_90, HR\_170) the effective measurement time per sky position is  $9 \cdot t_{\text{expo}}$  (C100) or  $4 \cdot t_{\text{expo}}$  (C200), respectively. For Cep\_90 and Cep\_170, which were oversampled in one direction only, the effective measurement time is  $2 \cdot t_{\text{expo}}$  for a subset of the map points.

Region	Cepheus		Draco Nebula (HR 6132)		Zodiacal Background Field		North Galactic Pole
	Cep_90	Cep_170	HR_90	HR_170	M03_90	M03_180	NGP_180
$\lambda_{\text{ref}}$ ( $\mu\text{m}$ )	90	170	90	170	90	180	180
Raster points	$9 \times 13$	$7 \times 14$	$12 \times 8$	$6 \times 4$	$12 \times 12$	$9 \times 9$	$15 \times 15$
Raster steps	$138'' \times 92''$	$180'' \times 92''$	$46'' \times 46''$	$92'' \times 92''$	$135'' \times 135''$	$180'' \times 180''$	$180'' \times 180''$
Field area	$20'.7 \times 20'.7$	$21'.0 \times 23'.0$	$10'.7 \times 7'.7$	$10'.7 \times 7'.7$	$27'.1 \times 27'.1$	$27'.1 \times 27'.1$	$45'.1 \times 45'.1$
$t_{\text{expo}}$ (s)	24	24	40	138	22	26	32
$\langle B \rangle$ ( $\text{MJy sr}^{-1}$ )	21.0	54.6	3.5	3.6	4.0	2.6	2.4
$BR$ ( $\text{MJy sr}^{-1}$ )	13.4 - 26.3	34.8 - 73.8	3.1 - 4.5	3.2 - 4.4	3.1 - 5.1	2.3 - 2.9	2.0 - 2.9
$\sigma_{\text{inst,sp}}$ (mJy)	7	21	1	1	6	7	9
$\sigma_{\text{inst,red}}$ (mJy)	17	46	2	4	5	4	5
$N_{\text{meas}}$ (mJy)	37	264	3	110	10	16	15
<b>N (mJy)</b>	<b>28</b>	<b>256</b>	<b>1</b>	<b>109</b>	<b>6</b>	<b>13</b>	<b>9</b>
$N_{\text{H\&B}}$ (mJy)	80	1636	5	28	7	20	17
$P_0$ ( $\text{Jy}^2 \text{sr}^{-1}$ )	$1.9 \cdot 10^5$	$1.6 \cdot 10^6$	$7.2 \cdot 10^3$	–	$4.0 \cdot 10^3$	$2.2 \cdot 10^3$	$2.3 \cdot 10^3$
$\alpha(d_0)$	-2.8	-3.6	-2.7	–	-0.5	-1.8	-2.0

4, NGP, one of the faintest regions near the north galactic pole selected for studies of the extragalactic background emission (Mattila et al. in preparation).

The observations were performed at  $90 \mu\text{m}$  with the C100 array ( $3 \times 3$  pixels) and at 170 and  $180 \mu\text{m}$  with the C200 array ( $2 \times 2$  pixels) of ISOPHOT. The raster mode of the Astronomical Observation Template (AOT) P22 (Klaas et al. (1994)) was used with the filters C\_90, C\_160 and C\_180, respectively. The rasters were performed in the spacecraft ( $Y, Z$ ) coordinate system which is parallel to the edges of the detector arrays. Observational details are given in Table 1.

### 3. Data reduction and calibration

ISOPHOT Interactive Analysis PIA<sup>1</sup> versions 5 and 6 (Gabriel et al. 1997b) extended by our own IDL routines were used to correct for instrumental effects, which is crucial for an analysis of background fluctuations. There are glitches by cosmic particles and flat-field artefacts impacting the power analysis at high spatial frequencies. Signal transients due to flux steps between the individual raster points can smooth out spatial structures. Detector switch-on effects introduce longer term drifts, introducing a systematic brightness pattern in the final maps. For a comparison of the absolute values of the structure noise and power spectra with the predictions by Helou & Beichman (1990) (Eq. (4)) the absolute brightness calibration is important, too. Most of our conclusions presented in this paper are, however,

not affected by absolute calibration uncertainties, but only by the stability of the calibration over the measurement time.

For the deglitching the PIA double stage deglitcher on ramp and signal level was used. For each field the deglitching parameters were optimised such to remove distinct signal excursions but preserving small-scale fluctuations of the signal.

Transient drifts were observed only at the very beginning of the measurements due to the detector switch-on effect. Using the Mann algorithm (Gabriel et al. 1997a) to discard these disturbed data points reduced the effective measurement time only marginally.

The signal time series of all pixels or the whole measurement time were inspected visually in order to determine long term detector responsivity drifts. A small monotonic drift with a signal difference of 5 % of the mean value between minimum and maximum was found which could be corrected for by fitting a linear baseline to the time series and scaling the signal values accordingly.

For the flat-field correction two different methods were chosen depending on the raster step size parameters. For those maps performed in the oversampling mode in both directions the redundancy information by multiple pixel coverage could be used to construct the flat-field. In the other cases a statistical flat field was applied. This method is based on the assumption that on average neighbouring detector array pixels receive the same flux. Fig. 1 shows an example applied to the Cepheus field. With some dynamic range in signal it is possible to correlate the signals of each individual pixel with those of the other ones. From the slope and the offset of those parts which correlate linearly the flat-field correction parameters were derived. For fields with al-

<sup>1</sup> PIA is a joint development by the ESA Astrophysics Division and the ISOPHOT consortium led by the Max-Planck-Institut für Astronomie, Heidelberg.

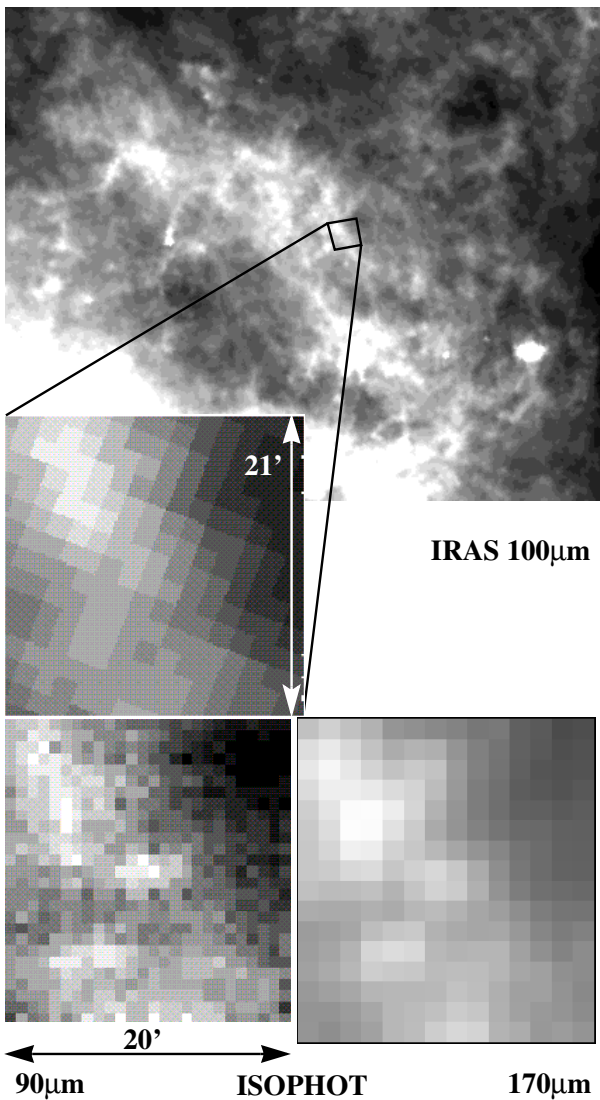


**Fig. 2.** IRAS Sky Survey Atlas (ISSA, Wheelock et al. (1994))  $100\ \mu\text{m}$  image of the Cepheus Flare with enlargement of the area covered by our observations (2 upper panels). Below: ISOPHOT  $90$  and  $170\ \mu\text{m}$  images of the same insert centred on  $(RA, DEC)_{J2000} = (21^{\text{h}}36^{\text{m}}31^{\text{s}}.9, +70^{\circ}34'10''.9)$ ,  $(l, b) = (108^{\circ}03, +13^{\circ}57)$ .

most no dynamic range the ratio of the median brightness values was taken to achieve a flat field.

The remaining fluctuations after these corrections are due to the sky brightness fluctuations and instrumental noise (photon, read-out noise, faint glitches by cosmic particles and responsivity variations on short time scales following ionizing particle hits). To estimate the instrumental noise the measurement time of a map was split into two halves per raster point. For each time interval we derived one map. From the differences of the values in the two maps we estimated the mean standard deviation. The results for each map in units of flux densities integrated over the solid angle of a detector pixel on the sky are listed as  $\sigma_{\text{inst,sp}}$  in Table 1.

We used the redundancy of the measurements to check the noise values. For the oversampled maps an estimate for the in-

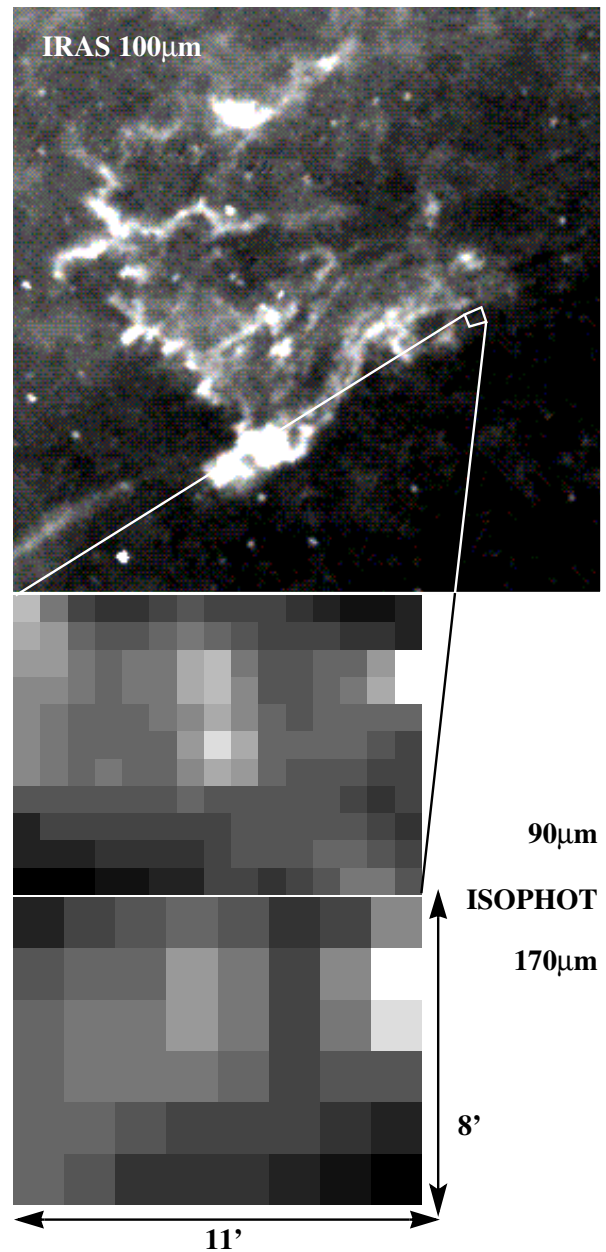


**Fig. 3.** ISSA  $100\ \mu\text{m}$  image of the Draco nebula (above). The ISOPHOT  $90$  and  $170\ \mu\text{m}$  observations of a small filament towards the star HR 6132 are displayed below. The centre position of the field is  $(RA, DEC)_{J2000} = (16^{\text{h}}23^{\text{m}}59^{\text{s}}.5, +61^{\circ}30'52''.0)$ ,  $(l, b) = (92^{\circ}58, +40^{\circ}95)$ . The central bright spot in the  $90\ \mu\text{m}$  map is the star HR 6132 (200 mJy).

strumental noise is obtained from the standard deviations of the mean brightness at each map point. These values are derived from the multiple measurements of the same position with various detector pixels. A representative estimate for each map point is achieved when averaging the standard deviations. The result for the instrumental noise in HR\_170 of 4 mJy is confirmed by additional staring observations of HR 6132 from the ISOPHOT calibration data base. A sequence of star-background observations was repeated four times with 64 s measurement time each

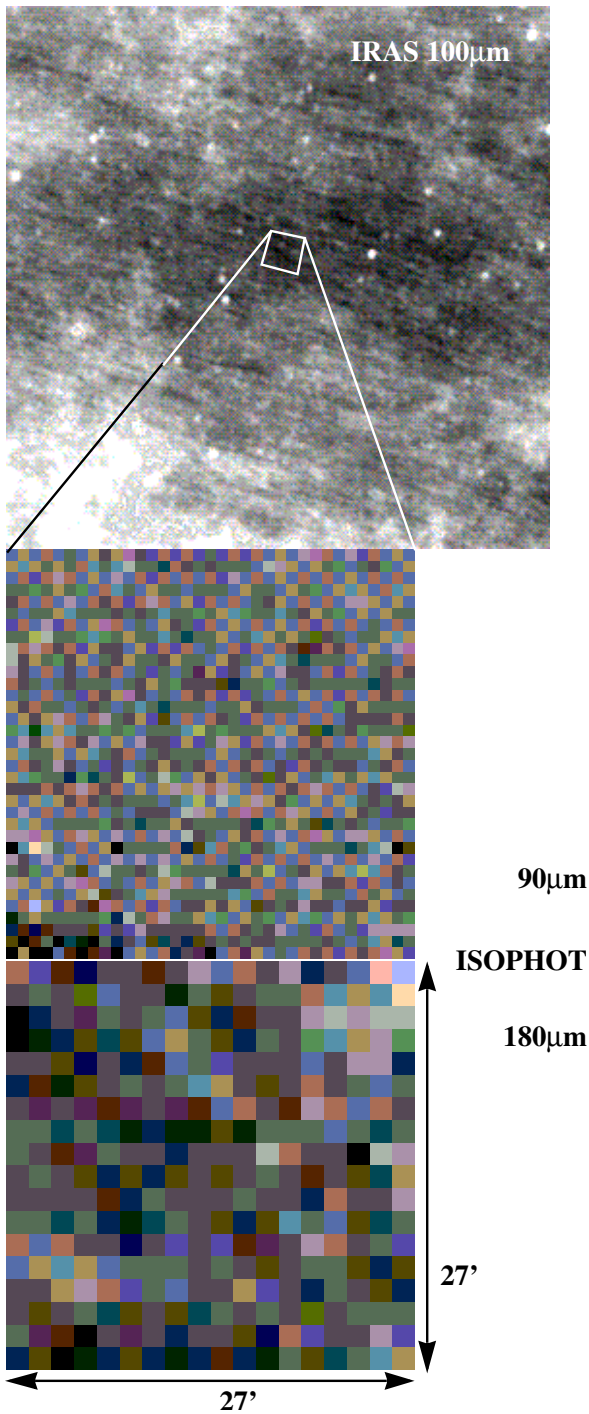


**Fig. 4.** ISSA  $100\ \mu\text{m}$  image of the region around M03 (above). The ISOPHOT  $90$  and  $180\ \mu\text{m}$  observations centred at  $(RA, DEC)_{J2000} = (13^{\text{h}}36^{\text{m}}12^{\text{s}}.4, +70^{\circ}34'53''.6)$ ,  $(l, b) = (117^{\circ}.65, +45^{\circ}.93)$  are displayed below.

step. From the variations of the values obtained towards the star an instrumental noise of  $5\ \text{mJy}$  is derived. For the non-oversampled maps additional independent linear scans across the centre of the fields are available providing the necessary redundancy. These scans were reduced in a similar way as the maps. The standard deviations per scan point and detector pixel

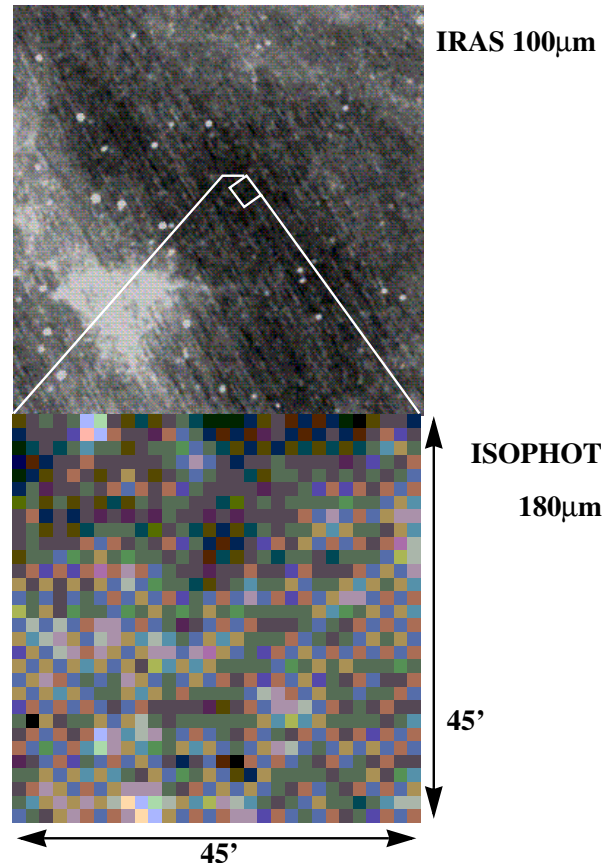


**Fig. 5.** ISSA  $100\ \mu\text{m}$  image of the region NGP near the north galactic pole. The ISOPHOT  $180\ \mu\text{m}$  observation centred at  $(RA, DEC)_{J2000} = (13^{\text{h}}42^{\text{m}}32^{\text{s}}.2, +40^{\circ}29'13''.6)$ ,  $(l, b) = (87^{\circ}.87, +72^{\circ}.98)$  is displayed below.

were derived from the mean difference between the map and scan brightness normalised to their mean values and accounting for the uncertainties introduced by the deviations of the mean values themselves. The results for each map in the same units as  $\sigma_{\text{inst,sp}}$  are listed in Table 1 as  $\sigma_{\text{inst,red}}$ .

For the maps M03\_90, M03\_180 and NGP\_180 the two estimates agree reasonably well, for the others the values derived from the redundancy analysis are larger than the values derived from the map splitting. In the case of the Draco nebula the very low instrumental noise is limited by systematic effects in the data. For the Cepheus field we suggest that systematic effects scaling with the total brightness (e.g. memory effects near bright sources) increase the instrumental noise. In all cases we adopt the larger value as a conservative estimate for the instrumental noise,  $\sigma_{\text{inst}}$ .

In general, the absolute calibration of ISOPHOT maps is done with respect to two bracketing internal calibration measurements. The internal reference sources are calibrated against celestial point source standards. We used recently derived effective solid angles to transfer the point source to the extended source calibration. These solid angles are  $0.67 \cdot 10^{-7}\ \text{sr}$  ( $90\ \mu\text{m}$ ),  $2.44 \cdot 10^{-7}\ \text{sr}$  ( $170\ \mu\text{m}$ ) and  $2.82 \cdot 10^{-7}\ \text{sr}$  ( $180\ \mu\text{m}$ ), respectively. We compared the resulting mean brightness values to values

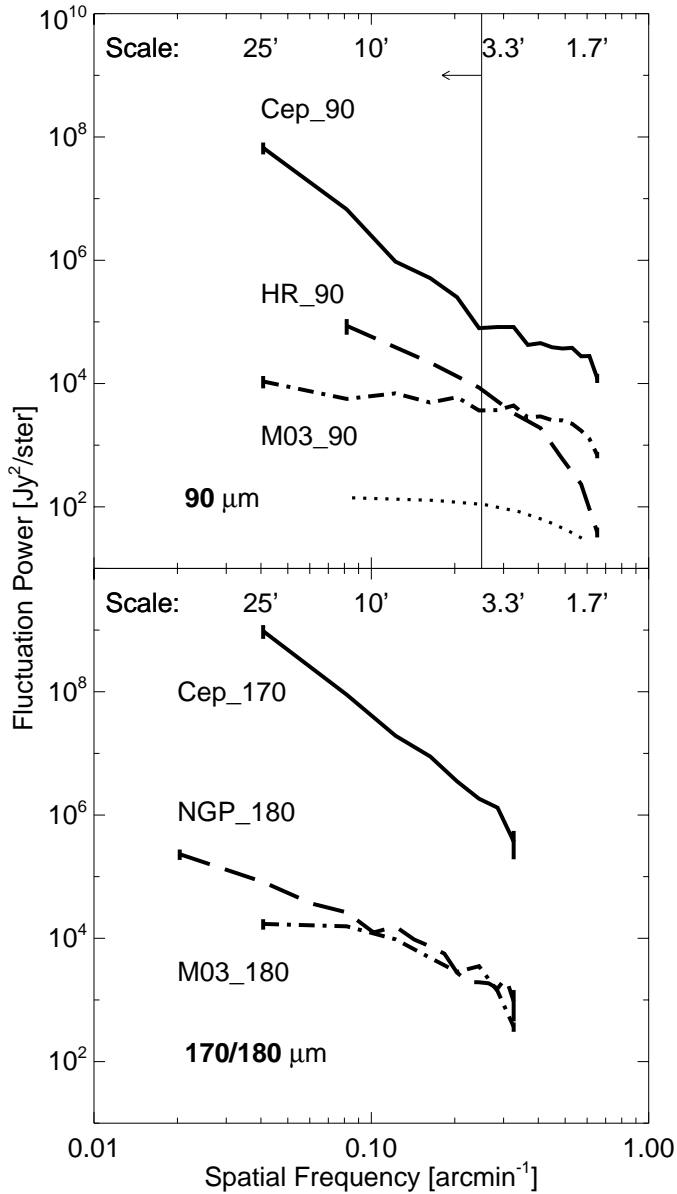


**Fig. 6.** Two-dimensional spatial frequency power spectra averaged over all azimuth angles. Representative errors ( $1\sigma_{\text{rms}}$ ) of the mean values are marked with bars at the end points of the spectra. The dotted curve in the upper panel shows the expected spatial frequency spectrum of a point source, i.e. the power spectrum of the instrument footprint arbitrarily scaled. The vertical line in the  $90\mu\text{m}$  plot marks the upper limit of the spatial frequency covered by IRAS.

derived from the DIRBE annual maps (Hauser et al. (1995)). The surface brightness values of the 60, 100, 140 and  $240\mu\text{m}$  DIRBE bands for COBE's nearest pointings to the field centres were interpolated in position and wavelength to derive the absolute flux values. At 60 and  $100\mu\text{m}$  the time variation of the zodiacal light brightness was checked. For all cases it was found that the average value in the annual maps is representative for the corresponding measurement period within the uncertainties. At longer wavelength the time variations are negligible compared to the measurement uncertainties derived from the weekly maps.

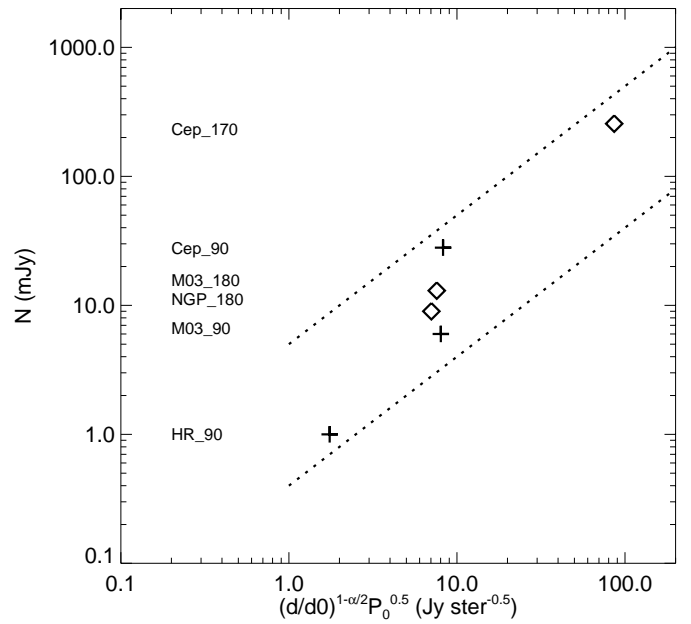


**Fig. 7.** Comparison of the derived background structure noise  $N$  with the values characterising the spatial structure following Eq. (3) with the values in Table 1. The dotted lines represent the theoretical predictions for two arbitrary scaling factors.

For the bright Cepheus filament the calibration derived from the FCS measurements and from DIRBE agree within 40% for the  $90\mu\text{m}$  and within 5% for the  $170\mu\text{m}$  map. At the time of writing this paper the calibration of the FCS is still preliminary, in particular the faint end of the calibration scale is not well covered with celestial standards, resulting in an uncertainty of about 50%. For the comparison with the noise predictions based on IRAS data and to keep consistency with results of similar analyses described in the literature (Bouchet et al. (1997)) we adopted therefore the method to calibrate our fields w.r.t. DIRBE.

The mean brightness values  $\langle B \rangle$  and the range in brightness,  $BR$ , i.e. the minimum and maximum brightness for each field, are listed in Table 1. The resulting cleaned and calibrated maps are presented in Figs. 2 to 5 beside IRAS  $100\mu\text{m}$  images of a larger area around the targets and, for the Cepheus filament, also of the area mapped with ISOPHOT.

#### 4. Structure noise in the observed fields

We computed the structure noise following Eq. (1). We considered each pixel in the maps as the on-source position and all possible pairs of pixels at  $\pm\theta$  as the corresponding background positions. The brightness differences were averaged for all possible  $\theta$  not regarding any dependence on the direction. The contributions from identical configurations, e.g. exchanging the background positions, were avoided. For all fields  $\theta_{\text{min}}$  and the measurement aperture width are determined by the pixel size  $46''$  for C100 and  $92''$  for C200. The results,  $N_{\text{meas}}$ , are listed in Table 1. These include a contribution from instrumental noise as determined in Sect. 3. The structure noise corresponding to  $\sigma_{\text{inst}}$  can be calculated assuming in Eq. (1) a brightness

distribution with zero mean and random fluctuation of rms amplitude  $1 \cdot \sigma_{\text{inst}}$ . It results in  $N_{\text{inst}} = \sqrt{2} \cdot \sigma_{\text{inst}}$ . As the sky fluctuation and instrumental noise contributions are statistically independent, they add up quadratically to the measured structure noise:

$$N_{\text{meas}}^2 \leq N^2 + 2 \cdot \sigma_{\text{inst}}^2 \quad (5)$$

Correcting for the instrument contribution assuming equality in Eq. (5) we compute the minimum structure noise ( $N$  in Table 1). Also listed are the cirrus noise values,  $N_{\text{H\&B}}$ , predicted by Helou & Beichman (1990) according to Eq. (4).

## 5. Power spectra

The software package GIPSY<sup>2</sup> was used to Fourier-transform the two-dimensional brightness distributions with periodogram normalisation (Press et al. (1992)). For the Fast Fourier Transform algorithm, each map was adapted to the nearest  $2^n \times 2^n$  pixels size. The algorithm implies a periodic repetition of the field in all sky directions introducing brightness jumps at the field edges. To avoid high frequency bias in the Fourier transforms due to these jumps the transitions were smoothed out by interpolating the data within a narrow strip along the map boundaries. These modified values either fill the extra field area due to the size adaptation and/or replace parts which show remaining non-linear detector switch-on drift effects. The highest spatial frequency for which the Fourier transform could be computed corresponds to a scale of  $2 \cdot \theta_{\text{min}}$ . The Fourier analysis of HR\_170 could not be performed because of too few data points.

Radial power spectra were derived from the square of the Fourier transforms averaged over all azimuth angles. Similar to previous results no analysis of anisotropies of the brightness distribution is intended here. Structures, like the filamentary elongation in the Cepheus field, mainly contribute to an azimuth modulation of the power at low spatial frequencies. The homogeneity, i.e. constant spatial characteristics for all points in the field, is a prerequisite for this and all similar analyses. Using the wavelet transform Abergel et al. (1996) support the validity of the assumption for cirrus clouds. The resulting spatial frequency power spectra are plotted in Fig. 6. Most of the spectra decrease with increasing spatial frequency following a single power law. HR\_90 shows a steepening of the spectrum at large frequencies. The fluctuation power,  $P_0$ , and slope of the radial spectrum at the reference scale  $d_0 = 4'$  are listed in Table 1. These values were determined by fitting a line to those parts of the spectra around  $d_0$  which show a constant spectral index.

## 6. Discussion

### 6.1. Limiting noise

Comparing the structure noise  $N$  with the instrumental noise  $\sigma_{\text{inst}}$  shows that for bright cirrus clouds the background fluctuations limit the point source detection for ISOPHOT C100

and C200 with observing times of  $\sim 20$  s per point. The small-scale brightness structure of the Cepheus filament in Fig. 2 is therefore dominated by emission fluctuations instead of detector noise. Also for faint fields the structure noise limits the flux density for detections with measurement times of the order of half a minute. For the field around HR 6132 the instrumental noise dominates at  $90 \mu\text{m}$ . The image at  $170 \mu\text{m}$  of the same region confirms, however, that the extended emission in the IRAS image resolves into distinct point-like sources. One of these can be identified with the emission from HR 6132, which is confused with another source. The structures in the low brightness fields M03 and NGP (Figs. 4 and 5) are not only due to instrumental noise. For M03\_90 and even more for M03\_180 and NGP\_180 parts of the emission fluctuations can be attributed to structures in the sky background.

### 6.2. Sky brightness structure at $180 \mu\text{m}$

The spatial frequency power spectra do not substantially change in the wavelength range beyond  $100 \mu\text{m}$  for scales down to  $3'$ . For the Cepheus and M03 fields the spectral index around  $180 \mu\text{m}$  is of the same order as the one derived at  $90 \mu\text{m}$  for scales down to  $3'$ . Therefore, the ISOPHOT observations substantiate one of the assumptions made by Helou & Beichman (1990) that the characteristic of the power spectra is independent of the wavelength. The similarity between the two wavelength bands suggests that in both the emission originates in the same or similarly distributed grain populations.

### 6.3. Power spectrum dependence on type of field

For the Cepheus filament at both wavelengths power laws are found with similar spectral index as those determined in the IRAS  $100 \mu\text{m}$  survey. At  $90 \mu\text{m}$  our analysis extends to even higher spatial frequencies. The filament can, therefore, be considered to represent a typical cirrus region with regard to the spatial structure.

The emission of the interstellar dust in the Draco nebula is resolved in a set of point-like features projected on diffuse cirrus emission. We interpret these point sources to be the reason for the reduced slope of the  $90 \mu\text{m}$  power spectrum. A comparison with the Fourier transform of a  $90 \mu\text{m}$  ISOPHOT point source footprint in Fig. 6 indicates a similar change of spectral index with spatial frequency. Therefore, areas where IRAS extended structures are resolved in point-like features can be recognised by a mixture of cirrus-cloud-like and typical point-source power spectra.

Similar as for the Cepheus filament the spatial frequency power spectra of M03 and NGP follow to Eq. (3). Here, however, the power spectrum is flatter than for the bright cirrus cloud. This characteristic which resembles more the one of random fluctuations indicates that the regions are probably almost free of cirrus structures. From Table 1 it can be seen that at least half of the fluctuation power is contributed by structure noise. Its origin is discussed in the following.

<sup>2</sup> Groningen Image Processing System, van der Hulst et al. (1980)

#### 6.4. Comparison with the spatial characteristics of the interstellar gas

We compare the far-infrared fluctuation power spectrum of the dust emission with the spatial characteristic of the interstellar gas. Possible contributors to the extended far-infrared brightness and its fluctuations are:

- Zodiacal light.
- Dust in the galactic cirrus clouds. A close correlation between the emission of the neutral gas (atomic and molecular) and in the far-infrared brightness of the dust down to the resolution of IRAS is found for many clouds. The Draco nebula shown in Fig. 3 is one example (Herbstmeier et al. (1993)).
- Dust in the smoothly distributed intercloud gas. This component consists of neutral and ionized hydrogen. Its emission decreases with galactic latitude (Boulanger & Pérault (1988)).
- Extragalactic background. The sum of the emission of randomly distributed extragalactic point-like sources which cannot be resolved. Estimates of the expected far-infrared flux of this component is given by Hauser (1996). Guiderdoni et al. (1997) predict the fluctuation spectrum due to this galaxy population.

According to Ábrahám et al. (1997) fluctuations of the zodiacal light are negligible. Its emission contributes to the value of the fluctuation power close to the spatial frequency 0 only and will therefore not be considered any further.

With ISOPHOT it is now possible to compare the fluctuation spectra of dust and gas in interstellar clouds, like the Cepheus flare, down to the  $1'$ -scale achieved with radio aperture synthesis telescopes in the 21 cm line. Crovisier & Dickey (1983) derived a spatial frequency power law spectrum of H I gas in the galactic plane with a spectral index of about  $-3$  (see also comments by Green (1993)). At mid galactic latitude Kalberla & Mebold (1983) found a similar spectrum with index  $-2.5$ . Kalberla & Stenholm (1983) report on fluctuation power law spectra with  $\alpha = -2.7$  obtained for parts of the Draco nebula at high galactic latitudes but only down to a scale of  $9'$ . Therefore, regardless of the galactic latitude, the interstellar H I gas shows spatial frequency spectra similar to those found for the far-infrared cirrus emission down to scales of about  $1'$ . This holds when considering the possible molecular hydrogen content in the Cepheus filament. Miesch & Bally (1994) demonstrate a similarity of the power spectra found in molecular gas with those of the H I component. The analogous spatial brightness fluctuation in gas and dust clouds, independent of their location, indicates that the small-scale structure in the emission is probably determined by similar kinematics (e.g. on scales of 0.2 pc for the Cepheus filament). For the interstellar gas turbulence is considered to be the reason for the specific fluctuation spectra.

Results of Kalberla & Stenholm (1983) imply that the diffuse neutral intercloud gas component shows similarly steep spectra as the clouds do. Parts of the ionized interstellar medium show spatial structure and a tight correlation with the H I dis-

tribution (Reynolds (1995)). In general Armstrong et al. (1995) found a steep density fluctuation spectrum for the interstellar plasma. It is therefore very unlikely that dust mixed with the diffuse neutral and ionized gas components determines the far-infrared fluctuations in the fields M03 and NGP. The emission of far-distant galaxies spread over the sky randomly could be the source for the structure noise in these fields. Recent models of the far-infrared emission of high-redshift galaxies by Guiderdoni et al. (1997) estimated their contribution to the fluctuation power spectrum. Taking into account that less than half of the power  $P_0$  in Table 1 is due to instrumental noise the range of  $1-2 \cdot 10^3 \text{ Jy}^2 \text{ sr}^{-1}$  for the fields M03 and NGP is of the same order as the predicted values of  $0.75-1.3 \text{ Jy}^2 \text{ sr}^{-1}$  by Guiderdoni et al. (1997). However, detailed studies similar to the one of Kashlinsky et al. (1996) have to be performed to examine the nature of the background emission seen in these faint emission fields (Mattila et al. in preparation).

#### 6.5. Consequences for subsequent space missions

With the values derived for our selected fields we can test the predictions by Helou & Beichman (1990). Eq. (4) describes qualitatively the results obtained here, moreover the values of  $N_{\text{H\&B}}$  and  $N$ , given in Table 1, agree within the order of magnitude. A closer correspondence is not expected, as the two basic assumptions are not valid for all fields. Neither the spectral index  $\alpha$  of our sample is confined to a small range around  $-3$  nor the results for  $P_0$  are closely related to the mean brightness values. In addition, this comparison depends on the absolute calibration as described in Sect. 3.

Dropping the assumptions made by Helou & Beichman (1990) we examine the relation between the structure noise and the characteristic measure of the spatial structure in the emission following Eq. (3). In particular, this relation is independent of any calibration scale uncertainty. For each field we plot in Fig. 7 the two quantities versus each other. Especially comparing the two results for the Cepheus region the data values follow quite well the trend predicted by Eq. (3) (see dotted lines). But, for similar characteristic measures of the cirrus structure the resulting structure noise can vary up to an order of magnitude. These deviations between the different fields can be explained considering that the proportionality factor depends on various parameters (Gautier et al. (1992)).

The trends indicate that for future 3 m class space telescopes (such as ESA's FIRST) faint source detection limits in the far-infrared imposed by cirrus noise are reduced by 1 – 2 orders of magnitude due to their improved spatial resolution. For smaller telescopes, such as ISO, high resolution mapping is the optimum observing strategy for the reliable detection of faint point sources. The AOTs P32 and P22 with oversampling promise the most sensitive results. Future space telescopes will not only gain by an increased telescope size but also from larger detector arrays, which allow to image the environment of faint sources simultaneously.

## 7. Conclusions

ISOPHOT far-infrared observations towards four fields of bright and faint far-infrared emission were performed in order to study their spatial characteristics.

- 1 We presented for the first time the analysis of the small scale structure measured in the  $180\ \mu\text{m}$  background emission.
- 2 Structure noise can determine the detection limit for the ISO observations of faint point sources in the far-infrared already for exposure times of 30 – 60 s.
- 3 At  $90\ \mu\text{m}$  ISO is able to reveal faint extended structures on scales of  $46''$ , i.e. on smaller scales compared to IRAS. The fluctuation power law derived from the IRAS measurements at  $100\ \mu\text{m}$  can be extended to higher spatial frequencies.
- 4 Down to scales of  $3'$  the cirrus emission at  $170\ \mu\text{m}$  shows a similar power law and spectral index as the  $90\ \mu\text{m}$  component. Either we see in both bands the emission of the same dust component, or the two different components show the same spatial distribution.
- 5 The far-infrared fluctuation spectra of the cirrus clouds can be traced down to the same scales as those derived for the interstellar gas. The power spectra of both components are very similar indicating a similar spatial behaviour.
- 6 Faint regions show a significant flattening of the spatial frequency power spectrum. Here, the structure noise of cirrus clouds becomes negligible. Fields dominated by point sources show the Fourier transform of the instrument's footprint on the sky.
- 7 For ISO and telescopes of similar sizes high-resolution mapping is the optimal observation mode to reliably detect faint point sources. Future infrared and sub-millimetre space missions with 3 m class telescopes will experience 1 – 2 orders of magnitude less cirrus confusion noise because of their higher spatial resolution. These surveys will also profit from future large detector arrays.
- 8 For the determination of an extragalactic background and similar analyses the estimate of the instrumental noise is essential. Here, a repetition of the observation optimized to assess the variations of the noise between the different detector pixels provides the necessary redundancy.

*Acknowledgements.* The work presented here profited from discussions with our colleagues at the ISOPHOT Data Centre of the MPIA, the ISOPHOT Instrument Dedicated Team at the ISO ground station and with the referee Dr. Jean-Loup Puget. Dr. Philippe Heraudeau contributed to the derivation of ISOPHOT's footprint on the sky. We appreciate discussions with Drs. Charles Beichman, Alain Abergel and Ernst Kreysa. ISOPHOT and the Data Centre at the MPIA, Heidelberg, are funded by the Deutsche Agentur für Raumfahrtangelegenheiten DARA and the Max-Planck-Gesellschaft.

## References

Abergel A., Boulanger F., Delouis J.M., et al., 1996, A&A 309, 245  
 Abraham P., Leinert C., Lemke D., 1997, A&A 328, 702  
 Armstrong J.W., Rickett B.J., Sprangler S.R., 1995, ApJ 443, 209  
 Boggess N.W., Mather J.C., Weiss R., et al., 1992, ApJ 397, 420

Bouchet F.R., Gispert R., Puget J.-L., 1997, The mm/sub-mm foreground and future CMB space missions, in: Proc. of the Moriond Conf. 1997, in press  
 Boulanger F., Péroul M., 1988, ApJ 330, 964  
 Crovisier J., Dickey J.M., 1983, A&A 122, 282  
 Désert F.X., Boulanger F., Puget J.L., 1990, A&A 237, 215  
 Gabriel C., Haas M., Heinrichsen I., Tai W.-M., 1997a, PIA User Manual Version 6.1  
 Gabriel C., Acosta-Pulido J., Heinrichsen I., et al., 1997b, Development and capabilities of the ISOPHOT Interactive Analysis (PIA), in: Proc. of the 5th International Workshop on "Data Analysis in Astronomy", Erice, Italy, in press  
 Gautier III T.N., Boulanger F., Péroul M., Puget J.L., 1992, AJ 103, 1313  
 Green D.A., MNRAS 262, 327  
 Guiderdoni B., Bouchet F.R., Puget J.-L., Lagache G., Hivon E., 1997, Nat 390, 257  
 Hauser M.G., Kelsall T., Leisawitz D., Weiland J., 1995, COBE Diffuse Infrared Background Experiment (DIRBE) Explanatory Supplement, Version 2.0  
 Hauser M.G., 1996, Searching for the Cosmic Infrared Background, in: Dwek E. (ed.), Unveiling the Cosmic Infrared Background, Proc. of COBE Workshop, American Institute of Physics  
 Helou G., Beichman C.A., 1990, The confusion limits to the sensitivity of submillimeter telescopes, in: From Ground-Based to Space-Borne Sub-mm Astronomy, Proc. of the 29th Liège International Astrophysical Coll., ESA Publ., p. 117  
 Herbstmeier U., Heithausen A., Mebold U., 1993, A&A 272, 514  
 Kalberla P.M.W., Mebold U., 1983, Mitt. Astron. Ges. 58, 101  
 Kalberla P.M.W., Schwarz U.J., Goss W.M., 1985, A&A 144, 27  
 Kalberla P.M.W., Stenholm L.G., 1983, Mitt. Astron. Ges. 60, 397  
 Kashlinsky A., Mather J.C., Odenwald S., 1996, ApJ 473, L9  
 Kessler M.F., Steinz J.A., Anderegg M.E., et al., 1996, A&A 315, L27  
 Klaas U., Krüger H., Heinrichsen I., Heske A., Laureijs R., 1994, ISOPHOT Observer's Manual, Version 3.1, ESA Publ.  
 Kun M., 1997, submitted to A&A  
 Lemke D., Klaas U., Abolins J., et al., 1996, A&A 315, L64  
 Low F., Beintema D.A., Gautier F.N., et al., 1984, ApJ 278, L19  
 Miesch M.S., Bally J., 1994, ApJ 429, 645  
 Press W.H., Teukolsky S.A., Vetterling W.T., Flannery B.P., 1992, Numerical Recipes in C, Cambridge University Press, 2nd edition  
 Puget J.-L., 1992, Interstellar Medium, in: Erennaz T., Kessler M.F. (eds.), Infrared Astronomy with ISO, Nova Science Publishers, New York, p. 271  
 Reynolds R.J., Tuft S.L., Kung D.T., et al., 1995, ApJ 448, 715  
 van der Hulst J.M., Terlouw J.P., Begeman K.G., 1992, GIPSY, in: Worall D.M., Biemesderfer C., Barnes J., Astronomical Data Analysis Software and Systems I, ASAP Conf Ser. 25, p. 131  
 Wheelock S.L., Gautier T.N., Chillemi J., et al., 1994, IRAS Sky Survey Atlas Explanatory Supplement, JPL Publ. 94-11 (Pasadena:JPL)